Electronic switching by metastable polarization states in $BiFeO_3$ thin films

Ye Cao,[1,2] Qian Li,[1] Mark Huijben,[3] Rama K. Vasudevan,[1] Sergei V. Kalinin,[1] and Petro Maksymovych[1,*]
[1]*Center for Nanophase Materials Science, Oak Ridge National Laboratory, Oak Ridge, Tennessee 37831, USA*
[2]*Department of Materials Science and Engineering, University of Texas at Arlington, Arlington, Texas 76019, USA*
[3]*University of Twente, Faculty of Science & Technology, 7500 AE Enschede, The Netherlands*

(Received 22 April 2018; published 4 September 2018)

We present an approach to control resistive switching in metal-ferroelectric contacts using a radially symmetric electric field. In ferroelectrics with significant polarization along the corresponding field lines, the field above a critical threshold will induce polarization discontinuity, a corresponding nanoscale volume of space charge, and a conducting junction. We demonstrate this principle using nanoscale polarization switching of a conventional (001)-oriented thin film of $BiFeO_3$. Without any optimization, the conducting state created in this regime of resistive switching exhibits local currents of ∼1–10 nA, approaching the ∼100 nA threshold required for device implementation [J. Jiang *et al.*, Nat. Mater. **17**, 49 (2018)]. The corresponding electronic function is that of a volatile resistive switch, which is directly compatible with neuristor functionality that encodes the functioning basis of an axon [M. D. Pickett *et al.*, Nat. Mater. **12**, 114 (2013)]. Phase-field modeling further reveals that in the strongly charged local configuration, $BiFeO_3$ locally undergoes a rhombohedral-tetragonal (R-T) phase transition, in part due to substantial piezoelectric expansion of the lattice. The estimated local charge density can be as high as $\sim 10^{21}$ cm^{-3}, which would be extremely difficult to achieve by conventional doping approaches without altering other material properties. Therefore, this method for creating stable and reproducible strongly charged ferroelectric junctions enables more systematic studies of their physical properties, such as the possibility of structural and electronic phase transitions, and it can lead to new ferroelectric devices for advanced information functions.

DOI: 10.1103/PhysRevMaterials.2.094401

I. INTRODUCTION

Ferroelectric polarization has historically preceded resistive switching [1] as a material-specific mechanism to store information in two-terminal devices, including the development and practical utilization of ferroelectric memories [2]. Over the past decade, many attempts have been made to couple ferroelectric and resistive switching so as to create bi- and multistable electronic memory elements [3–7], controlled by the intrinsic energy landscape of the ferroelectric order parameter rather than defect-mediated electroresistive phenomena [8]. Much attention has been drawn to the phenomenon of conducting ferroelectric domain walls, most notably in lead zirconate and bismuth ferrite [9–11]. In parallel, several efforts have pursued resistive switching in metal-ferroelectric junctions, including Schottky contacts [3,7,12], tunneling contacts [3,13], and tunnel junctions [5,6,14], where the electron potential in the junction is modulated by various properties of ferroelectric polarization.

An important task for fundamental and practical developments of polarization-controlled electroresistance is the development of reliable and reproducible methods to create conducting ferroelectric entities. Charged domain walls, for example, are formed when polarization is discontinuous across the wall [15,16]. They may have extraordinarily large energies (up to 100-fold larger compared to uncharged walls [15]), which makes them intrinsically unstable. Strongly charged domain walls will therefore prefer to reconstruct to reduce or remove the built-in charge (as was demonstrated in artificial domain-wall junctions in $BiFeO_3$ [17]). In some materials, such as (hybrid) improper ferroelectrics, charged domain walls are stabilized by the energy of the primary ferroelastic order parameters as well as the additional electrostatic screening [18,19]. However, these effects are only limited to a very specific material class, whereas spontaneous polarization of improper ferroelectrics is at least an order of magnitude smaller compared to proper ferroelectrics, again leading to weakly charged domain walls. Ferroelectric tunnel junctions, on the other hand, are constrained by the detrimental effect of dimensional size effects which suppress ferroelectricity at the nanoscale [20]. Steady progress is being made along these directions, but new phenomena which do not necessarily rely on conducting walls and manifest in robust 10–50 nm ferroelectric films would be desired. In particular, they may lead to more definitive answers to numerous open questions regarding resistive phenomena in ferroelectrics, including the underlying mechanisms, the limits of scalability, deterministic approaches to control and tune the magnitude of the resistive switching, as well as device implementation.

Here we present a volatile resistive switching function of a conventional ferroelectric film that vividly demonstrates the utility of the polarization control of resistive currents. Specifically, we apply an electric field with a radially symmetric geometry [Fig. 1(a)] to a ferroelectric with a substantial in-plane polarization component [Fig. 1(b)]. Above a critical

*Corresponding author: maksymovychp@ornl.gov

 ©2018 American Physical Society

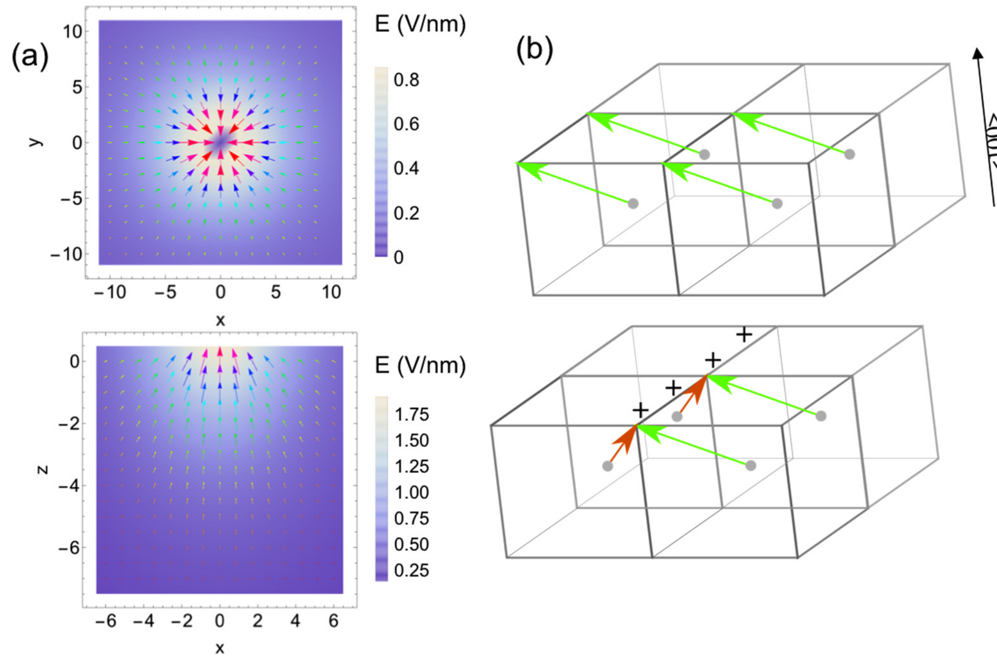

FIG. 1. (a) Radially symmetric electric field created by localized probe, whose potential distribution is modeled as $\frac{Ud}{\sqrt{x^2+(\frac{z}{\gamma}+d)^2}}$, where γ is the dielectric anisotropy, d is roughly proportional to the tip radius of the curvature (assumed = 10 nm), and U is the applied potential (here -4 V). (b) Schematic of polarization orientations in a (001)-oriented film of $BiFeO_3$, with initial polarization along the [−1 −1 1] direction. The simplest "in-plane" switching is a partially switched polarization component to the [1 −1 1] direction, creating a charged 71° domain wall.

threshold, the polarization will be realigned with the field. As a result, the polarization will become discontinuous at the center of the field distribution, causing a large density of static polarization charge to be accumulated in the material volume. In the specific case of $BiFeO_3$(100), one such possibility is a charged "head-to-head" 71° polarization domain wall [Fig. 1(b)]. This space-charge distribution will almost certainly change the conductivity of the ferroelectric film, by either accumulation of screening mobile carriers in the bulk volume of the film or by screening of the contact potential. Here we demonstrate the latter case. In one of the simplest implementations, that is almost ubiquitous today, the necessary field is created by a nanoscale biased metal probe in contact with a ferroelectric material. We also reveal that in this case, the field-induced process involves not only polarization reorientation, but also a local structural phase transition to tetragonal symmetry [21], while maintaining large space-charge density in the contact.

II. RESULTS

A 12-nm-thick (001)-oriented $BiFeO_3$ (BFO) film was deposited on 5 nm $La_{0.7}Sr_{0.3}MnO_3$ (LSMO) electrodes by pulsed-laser deposition (PLD) with reflection high-energy electron diffraction (RHEED) control (at 1023 K and $pO_2 =$ 200 mTorr for LSMO and 943 K and $pO_2 = 100$ mTorr for BFO [22]) followed by slowly cooling to room temperature in 1 atm of oxygen at ∼5 K/min. Characterization of the films from the same growth batch by transmission electron microscopy and x-ray ellipsometry was described in more detail in [23]. Good crystalline quality of $BiFeO_3$ is also ascertained by flat terraces [Fig. 2(a)], separated by steps of multiple unit-cell heights, which is quite typical for this material.

Scanning probe microscopy was carried out on the films introduced from the ambient environment into a vacuum chamber with no further processing [3]. The experiments utilized a modified Omicron VT-SPM, optimized for piezoresponse force microscopy and conductive atomic force microscopy measurements. All the measurements were carried out in ultrahigh vacuum, with a background pressure of $<2\times10^{-10}$ Torr. Variable temperature conductance measurements were carried out by heating the samples with a PBN heater connected to the sample stage with a copper braid. Local strain and current measurements were carried out with commercial Budget Sensor AFM probes (ElectriMulti75-G), in ultrahigh vacuum at room temperature. The measurements were not sensitive to the voltage sweep rates from 0.1 to 50 V/s.

Figure 2 shows a characteristic set of I-V curves [Fig. 2(b)] and simultaneously recorded local strain curves [Fig. 2(c)], obtained on a random location of the surface of the film. Electronic switching is evidenced by the abrupt increase of local current at the applied bias of slightly less than -4 V, by about two orders of magnitude from its initial value [blue in Fig. 2(b)]. On the reverse voltage ramp, the conducting trace [red in Fig. 2(b)] reverts back to the background value at a bias of about -2 V. This reversion is likewise abrupt and does not merely indicate the reduction of the measurable current below the noise level of the amplifier. Instead it corresponds to the back switching between conducting and insulating states of the film.

The cause of the electronic switching can be assigned to the ferroelectric properties of $BiFeO_3$ through careful inspection of the strain loops in Fig. 2(c). These loops have approximately piecewise linear shape, with discontinuities marking the abrupt change of spontaneous polarization. A ferroelectric

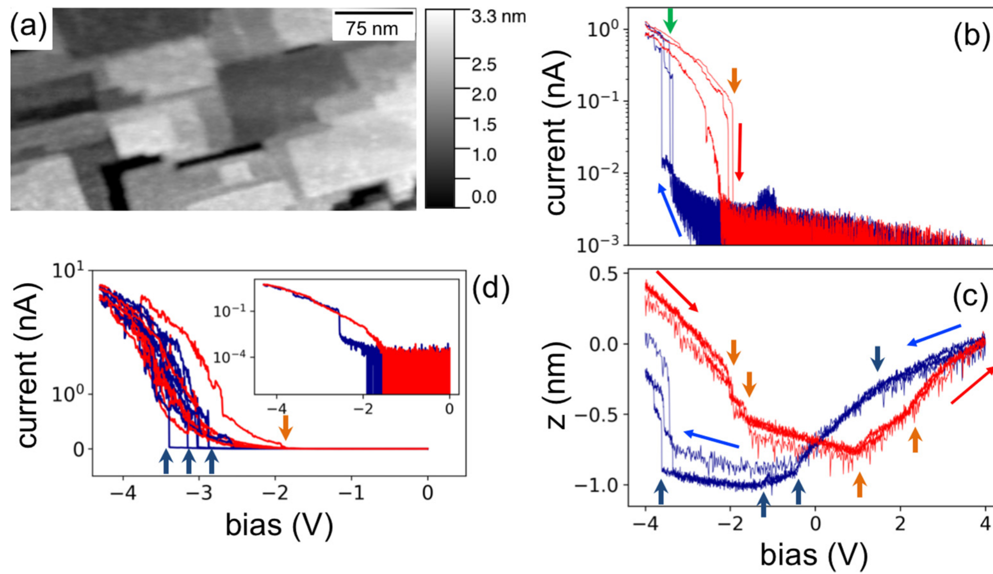

FIG. 2. (a) Topography of the 12 nm $BiFeO_3$ film. Simultaneous measurements of (b) local current and (c) strain in the $BiFeO_3$ film as a function of local voltage applied to the atomic force microscopy (AFM) tip. The strain loop in (c) exhibits discontinuities at the ferroelectric switching events at negative bias polarity, some of which also coincide with discontinuities in the I-V curve in (b). (d) I-V curves on a preswitched surface obtained with a bias ramp between 0 and −4.3 V. Blue and red colors correspond to forward and reverse direction of the bias ramp. Three, two, and four sequential sweeps are shown in panels (b)–(d), respectively. The inset of (d) shows one sweep.

film with uniaxial polarization allows two oppositely oriented polarization states, in which case each branch of the strain loop will exhibit just one discontinuity (Fig. S1 of the Supplemental Material [24]), marking the instance of polarization reversal [3]. However, the (001)-oriented $BiFeO_3$ film exhibits at least two discontinuities along both forward and reverse branches of the strain hysteresis [Fig. 2(c); Fig. S1 of the Supplemental Material [24]), indicating several sequential events of polarization switching. Using the schematic in Fig. 1(b), it is straightforward to hypothesize that the two switching events should correspond to the out-of-plane switching of the polarization orientation (either 71° or 109°), followed by an in-plane switching owing to the ⟨111⟩ directionality of the polarization (likewise either 71° or 109° reorientation of the polarization vector).

Purely in-plane switching has been demonstrated in several previous studies [17,21]. It is not immediately clear that an out-of-plane switching should precede in-plane switching [25], with the energies determined by both the switching pathways and the final configurations. Furthermore, neither out-of-plane nor in-plane reversal should necessarily create polar discontinuities [17]. In fact, it was previously demonstrated that careful control over the trajectory of a moving and biased tip can deterministically switch the in-plane polarization over microscopic length scales, creating “ferroelectric vortex” domains with uncharged domain walls [17].

However, for a stationary biased tip, the radially symmetric electric field will eventually force the creation of a polar discontinuity, by symmetry. This configuration will necessarily exhibit higher energy due to the bound charge, and it may also enable carrier transport across the film, either by lowering the barrier to carrier injection or by creating a conduction pathway across the film. This is why we observe both electronic switching, electronic back switching, and significant conductivity only in the respective window of higher applied voltages. This argument is also supported by observing the conductance of a purely in-plane switching trajectory, where the out-of-plane polarization has been preswitched along the normal field component in a separate scan cycle before measuring the conductance [Fig. 2(d)]. The voltage ramp then starts at 0 V and extends only into the negative branch to single out only one of the polarization reorientation mechanisms. One clearly observes an abrupt increase of the local current, to approximately the same level as in the symmetric ramp in Fig. 2(b). However, the back switching is less clear in this case, as it tends to occur close to the measurement noise level. We note that resistive switching is well reproducible at each location of the surface (Fig. S2 of the Supplemental Material [24]).

The above picture provides a qualitative account of the observed processes, and it should hold for any film with a significant in-plane polarization. Given the intricacies of local ferroelectric switching in $BiFeO_3$ [21,25], we turn to the well-established methodology of phase-field modeling to identify possible electrostatic effects that emerge at larger electric field. As seen in Fig. 3(a), local polarization switching involves the occurrence of all eight allowed polarization vectors above a critical field that is consistent with earlier observations [21,25]. Four “quadrants” [−1, 1, −1], [−1, −1, −1], [1, 1, −1], and [1, 1, −1] orientations intersect at the center of this switched configuration, so that the in-plane components of the polarization vectors all point away from the center and along the field lines, in agreement with the general logic outlined above. It turns out that in $BiFeO_3$, it becomes energetically favorable to orient the polarization vector along the ⟨001⟩ orientation, essentially forming a nanoscale volume of a pseudotetragonal phase under the tip [Fig. 3(b)]. Note that the rhombohedral-tetragonal (R-T) transition is delayed in voltage

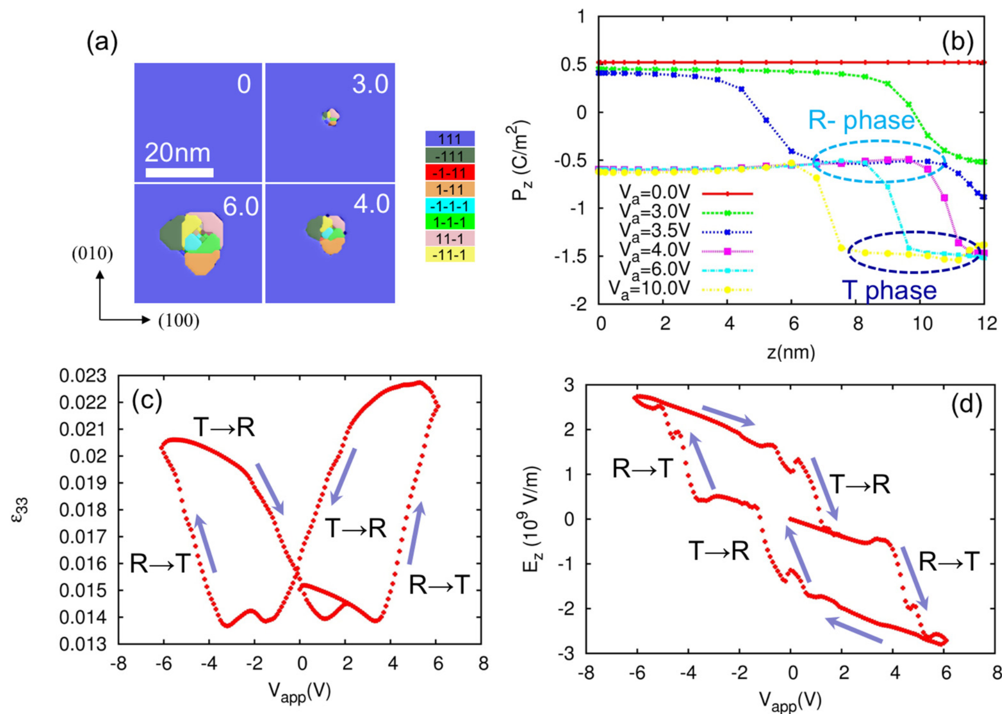

FIG. 3. Phase-field modeling of polarization switching in 12-nm-thick (001)-oriented $BiFeO_3$ thin film. (a) In-plane (x-y) polarization switching of eight emerging domain variants for increasing tip bias. (b) Evolution of the out-of-plane polarization (P_z) along the z direction extending from the center of the tip normal to the film's bottom interface. The initial positive $P_z(\sim 0.52\,\mathrm{C/m^2})$ was first switched to negative ($\sim -0.52\,\mathrm{C/m^2}$) near the tip and propagates through the film thickness when the bias is below 3.0 V. Above 4.0 V, an additional rhombohedral (111) to pseudotetragonal (001) phase transition occurs ($P_z \sim -1.5\,\mathrm{C/m^2}$). (c) Strain-bias hysteresis (butterfly) loop associated with the localized switching. (d) The localized electric field (E_z) under the tip as a function of sweeping tip bias. Discontinuities in the slope of $E_z = f(V)$ can be observed, which are associated with the R-T phase transition that induces large polarization bound charges.

by about one volt relative to the out-of-plane switching in the phase-field calculation [Fig. 3(b)], in qualitative agreement with the experiments in Fig. 2. This tip-induced R-T transition was previously determined by observing a modification of the elastic properties of the tip-surface junction [21], and was hypothesized earlier [26].

Figure 3(c) shows the calculated evolution of the local strain along the polarization switching. The R-T switching is associated with a very large expansion of the local volume directly under the probe, which is again qualitatively consistent with the strain loops in Fig. 2(c). The volume of the T phase is metastable and it reverts back to the R phase before the bias polarity switches sign, likewise in agreement with the experiment. The R-T transition occurs at both bias polarities. The predictions of the phase-field modeling point to the less abrupt appearance and disappearance of the T phase, but it is clear that not all properties of the experimental junction can be described by modeling, particularly the pinning and the lattice potentials.

Although the R-T configuration is more complicated than a simple polar discontinuity, anticipated to occur for a radially symmetric field (Fig. 1), it readily creates a large local density of bound polarization charge, as seen in Fig. S3 (see Supplemental Material [24]), which plots $-\nabla P$ as a function of the distance from the tip-surface junction. The charge is concentrated directly under the tip and achieves a remarkable density of $\sim 10^{21}\,\mathrm{cm^{-3}}$, approximately comparable to the doping threshold for pseudotetragonal ferroelectric instability in Ca-doped $BiFeO_3$ [27]. Of course, in the case of electrostatic doping, the transition is completely reversible. The charge is primarily concentrated around the T-phase region, which itself is localized in the region of the maximum field.

The simplest mechanism by which a large density of polarization charge increases the junction conductance is through the effect of local band bending in the contact region. This is essentially the same mechanism as in the formation of a Schottky barrier at the contact to a doped semiconductor, albeit with potential screening provided by the polarization charge rather than due to an ionized dopant. By analogy with a reverse-biased Schottky barrier, the enhancement of the electric field in the junction, due to space-charge screening, enhances or enables Schottky emission or Fowler-Nordheim tunneling into the conduction band (or valence band for opposite polarity and sign of space charge). As shown in Fig. 3(d), field enhancement is indeed quite dramatic when the T phase occurs, approaching near-breakdown values for most dielectric materials. It should be noted that this R-T phase transition can be realized under both bias polarities [Fig. 3(d)], although experimentally we observe conductance only at one polarity, most likely due to a large difference in the Schottky barrier height at opposite interfaces.

The analysis of the I-V curves in the high-field conducting state is shown in Fig. 4. Given the relatively broad distribution of switching thresholds across the surface, averaging over the

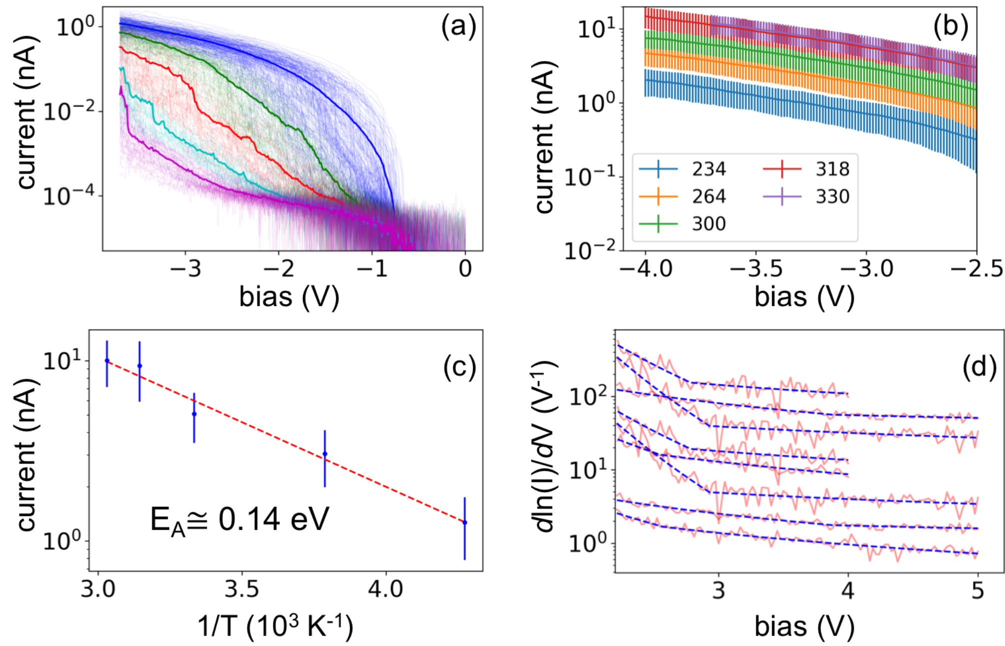

FIG. 4. Analysis of voltage scaling and temperature dependence of I-V curves on the 12 nm $BiFeO_3$ film. (a) 400 I-V curves obtained on a grid of 20×20 points at 330 K. The colors correspond to a cluster of I-V curves identified using agglomerative clustering with the Ward variance minimization algorithm as implemented in SCIPY python library. The thick solid lines mark the mean value of current for each cluster. (b) Temperature dependence of mean-clustered values of current corresponding to the conducting states. Individual colors correspond to measurement temperatures in K, as shown in the legend. (c) The Arrhenius plot of current at a bias of −3.45 V. (d) Voltage scaling of the individual I-V curves as discussed in the text.

whole dataset in this case produces unphysically larger error bars, far exceeding the measurement noise or the intrinsic scatter of the data points. We have therefore employed statistical clustering methods to select the I-V curves corresponding to the conducting states [Fig. 4(a)] and to differentiate them from (the minority) of I-V curves due to unswitched insulating regions as well as I-V curves that have partial or erratic switching behavior. Specifically, we utilized agglomerative clustering to the region of the I-V curve between −2.5 and −3.5 V into five clusters (selecting more or fewer clusters did not significantly change the outcome for the most conducting state) (see Figs. S4(a)–S4(c) in Supplemental Material [24]). This automated routine has also allowed us to reliably quantify the levels of measured current, and carry out reproducible temperature-dependent characterization of the conducting states, as shown in Figs. 4(b) and 4(c). The conduction was determined to be thermally activated with a barrier of ∼0.14 eV, indicating shallow trapping somewhere at the current-limiting step (e.g., trap-assisted tunneling [28,29]).

The I-V curves are strongly nonlinear, with the slope of the normalized differential conductance [$\frac{d\ln(I)}{dV}$] ranging from 1.5 to 2.5 (Fig. S4(d) in Supplemental Material [24]). Based on previous studies and strong asymmetry of the I-V curves, the data are most consistent with tunneling mechanisms [30]. The overall picture is therefore similar to carrier injection in $Pb(Zr_xTi_y)O_3$ [3] and many other ferroelectrics. Although the details of this process remain to be fully understood, any tunneling mechanism scales exponentially with the electric field in the tunneling region, and therefore will be enhanced by the occurrence of a large density of polarization charge as described above.

III. DISCUSSION

In the case of (001)-oriented $BiFeO_3$, the in-plane component exists due to the ⟨111⟩-direction of the polarization axis. Above a critical threshold field, the in-plane component is reversed [Fig. 1(a)], creating a “head-to-head” or “tail-to-tail” configuration, where polarization is discontinuous across the domain wall. The energy that stabilizes such domain wall, or more generally the polarization discontinuity at the domain wall, is provided by the applied electric field. Increasing the electric field only further stabilizes the configuration (and possibly increases the spatial extent of the polar discontinuity), enabling a robust and stable conduction. Moreover, the radially symmetric field “traps” the polar discontinuity, allowing one to create conducting entities on demand and, at the same time, to minimize the spatial extent of the conducting junction and prospectively leading to much greater device density. This is in contrast to strongly conducting domain walls of ferroelectric nanodomains in PZT [31], where a large conductance was measured, although both the tilt angle of the domain wall [32] (responsible for the occurrence of bound polarization charge) as well as the position of the domain wall itself were both transient, and disappearing from the junction upon an increased bias. In the absence of the field, the charged domain wall becomes unstable, the polarization configuration reverses, and the electronically insulating state is restored. As a result, the electronic function of such a geometry is that of a volatile switch which switches between distinct electronic states at the same voltage polarity. Curiously, electronic switching of this type is reminiscent of current-controlled Mott metal-insulator switches [33], which may find their application as a neuristor

circuitry. In light of the recent measurements of the R-T phase transition in $BiFeO_3$ on nanosecond timescales [34], such switches can also potentially operate on fast timescales, particularly if the volume of the film can be reduced to the nanoscale dimension.

We would like draw a brief comparison to the recent work by Jiang *et al.* [35], reporting on the implementation of electronic memory function using transient conducting domain walls. Similarly to our work, the authors reported volatile resistive switching in $BiFeO_3$. However, the device geometry involved two electrodes on the surface of a $BiFeO_3$ film, where the electrode gap with dimension of few 100 nm would create an in-plane electric field, and correspondingly switch the $BiFeO_3$ into a domain with charged domain walls. In our case, discontinuous polarization configuration is achieved in an ultrathin film with a field that has radial symmetry. Thus, although the IV curves in the two studies are remarkably similar, the detailed polarization configuration responsible for resistive switching is quite different—corresponding to extended charged domain walls in the device geometry, and a highly confined tetragonal configuration in our case. It seems feasible to propose that the R-T transition may also be occurring in the device geometry by Jiang *et al.*, so that the current is likewise controlled by a polar discontinuity at the interface, rather than the bulk volume of the material. Both of these configurations produce much more conducting entities with the resistance of ~50–100 MOhm, compared to 10–100 GOhm for as-grown domain walls [9,10,36].

Finally, we note that we do not assume the metallization of the charged region, which is the common proposal of explaining conductivity of ferroelectric domain walls [37,38]. We do not observe evidence of metallic conduction directly, suggesting that the volume associated with polarization discontinuity does not traverse the whole thickness of the film. Moreover, the current density is still very small and I-V curves indicate tunneling conductance, both pointing to contact-limited mechanisms. Our explanation for the enhanced conductance is therefore well aligned with our recent analysis of the field enhancement of the electronic conductance of as-grown extended domain walls in $BiFeO_3$ [13]. However, it is interesting to consider what happens if such switching can be achieved in films thinner than 12 nm, where the discontinuous region may connect top and bottom electrodes.

IV. CONCLUSION

In conclusion, we presented an approach to control resistive switching in ferroelectric films, using a radially symmetric electric field. Resistive switching is robust in the studied films of $BiFeO_3$ and yields conducting entities with local current in excess of 10 nA and spatial localization of a few tens of nm. The underlying mechanism behind resistive switching is a polar discontinuity created by reorientation of polarization vectors along the radially symmetric field. Given the anticipated generality of this mechanism, in-plane polarized ferroelectrics may be an intriguing alternative for eventual device prototypes incorporating polarization-controlled resistive switching, and coincidentally they will also be more robust toward a decreasing of the film thickness. In principle, when the film thickness becomes comparable to the extent of the polarization discontinuity, the current density should increase dramatically and the electronic structure within the polar discontinuity [39] may become directly accessible for transport measurements. Similar ideas may apply for other properties associated with strongly charged ferroelectric regions, such as electrochemical reactions and nonlinear dielectric properties.

ACKNOWLEDGMENTS

The work was supported by the U.S. Department of Energy, Office of Science, Basic Energy Sciences and Materials Sciences and Engineering Division (Y.C., R.K.V., S.V.K., P.M.). This research was conducted at the Center for Nanophase Materials Sciences, which is a DOE Office of Science User Facility.

[1] D. S. Jeong, R. Thomas, R. S. Katiyar, J. F. Scott, H. Kohlstedt, A. Petraru, and C. S. Hwang, Rep. Prog. Phys. **75**, 076502 (2012).
[2] J. F. Scott, Science **315**, 954 (2007).
[3] P. Maksymovych, S. Jesse, P. Yu, R. Ramesh, A. P. Baddorf, and S. V. Kalinin, Science **324**, 1421 (2009).
[4] E. Y. Tsymbal and H. Kohlstedt, Science **313**, 181 (2006).
[5] V. Garcia and M. Bibes, Nat. Commun. **5**, (2014).
[6] A. Chanthbouala, A. Crassous, V. Garcia, K. Bouzehouane, S. Fusil, X. Moya, J. Allibe, B. Dlubak, J. Grollier, S. Xavier, C. Deranlot, A. Moshar, R. Proksch, N. D. Mathur, M. Bibes, and A. Barthélémy, Nat. Nanotechnol. **7**, 101 (2012).
[7] P. W. M. Blom, R. M. Wolf, J. F. M. Cillessen, and M. P. C. M. Krijn, Phys. Rev. Lett. **73**, 2107 (1994).
[8] J. J. Yang, D. B. Strukov, and D. R. Stewart, Nat. Nanotechnol. **8**, 13 (2013).
[9] J. Seidel, L. W. Martin, Q. He, Q. Zhan, Y.-H. Chu, A. Rother, M. E. Hawkridge, P. Maksymovych, P. Yu, M. Gajek, N. Balke, S. V. Kalinin, S. Gemming, F. Wang, G. Catalan, J. F. Scott, N. A. Spaldin, J. Orenstein, and R. Ramesh, Nat. Mater. **8**, 229 (2009).
[10] J. Guyonnet, I. Gaponenko, S. Gariglio, and P. Paruch, Adv. Mater. **23**, 5377 (2011).
[11] P. Maksymovych, Nat. Nanotechnol. **10**, 571 (2015).
[12] T. Choi, S. Lee, Y. J. Choi, V. Kiryukhin, and S.-W. Cheong, Science **324**, 63 (2009).
[13] R. K. Vasudevan, Y. Cao, N. Laanait, A. Ievlev, L. Li, J.-C. Yang, Y.-H. Chu, L.-Q. Chen, S. V. Kalinin, and P. Maksymovych, Nat. Commun. **8**, 1318 (2017).
[14] D. J. Kim, H. Lu, S. Ryu, C.-W. Bark, C.-B. Eom, E. Y. Tsymbal, and A. Gruverman, Nano Lett. **12**, 5697 (2012).
[15] P. S. Bednyakov, T. Sluka, A. K. Tagantsev, D. Damjanovic, and N. Setter, Sci. Rep. **5**, 15819 (2015).
[16] B. M. Vul, G. M. Guro, and I. I. Ivanchik, Ferroelectrics **6**, 29 (1973).
[17] N. Balke, B. Winchester, W. Ren, Y. H. Chu, A. N. Morozovska, E. A. Eliseev, M. Huijben, R. K. Vasudevan, P. Maksymovych, J. Britson, S. Jesse, I. Kornev, R. Ramesh, L. Bellaiche, L. Q. Chen, and S. V. Kalinin, Nat. Phys. **8**, 81 (2012).
[18] Y. S. Oh, X. Luo, F.-T. Huang, Y. Wang, and S.-W. Cheong, Nat. Mater. **14**, 407 (2015).

[19] D. Meier, J. Seidel, A. Cano, K. Delaney, Y. Kumagai, M. Mostovoy, N. A. Spaldin, R. Ramesh, and M. Fiebig, Nat. Mater. **11**, 284 (2012).
[20] K. M. Rabe, editor, *Physics of Ferroelectrics: A Modern Perspective; with 24 Tables* (Springer, Berlin, 2007).
[21] Q. Li, Y. Cao, P. Yu, R. K. Vasudevan, N. Laanait, A. Tselev, F. Xue, L. Q. Chen, P. Maksymovych, S. V. Kalinin, and N. Balke, Nat. Commun. **6**, 8985 (2015).
[22] Y. H. Chu, T. Zhao, M. P. Cruz, Q. Zhan, P. L. Yang, L. W. Martin, M. Huijben, C. H. Yang, F. Zavaliche, H. Zheng, and R. Ramesh, Appl. Phys. Lett. **90**, 252906 (2007).
[23] P. Maksymovych, M. Huijben, M. Pan, S. Jesse, N. Balke, Y.-H. Chu, H. J. Chang, A. Y. Borisevich, A. P. Baddorf, G. Rijnders, D. H. A. Blank, R. Ramesh, and S. V. Kalinin, Phys. Rev. B **85**, 014119 (2012).
[24] See Supplemental Material at http://link.aps.org/supplemental/10.1103/PhysRevMaterials.2.094401 for supporting data and the details of the phase-field modeling.
[25] N. Balke, S. Choudhury, S. Jesse, M. Huijben, Y. H. Chu, A. P. Baddorf, L. Q. Chen, R. Ramesh, and S. V. Kalinin, Nat. Nanotechnol. **4**, 868 (2009).
[26] H. Bea, B. Ziegler, M. Bibes, A. Barthelemy, and P. Paruch, J. Phys.: Condens. Matter **23**, 142201 (2011).
[27] C.-H. Yang, J. Seidel, S. Y. Kim, P. B. Rossen, P. Yu, M. Gajek, Y. H. Chu, L. W. Martin, M. B. Holcomb, Q. He, P. Maksymovych, N. Balke, S. V. Kalinin, A. P. Baddorf, S. R. Basu, M. L. Scullin, and R. Ramesh, Nat. Mater. **8**, 485 (2009).
[28] F. Jiménez-Molinos, A. Palma, F. Gámiz, J. Banqueri, and J. A. López-Villanueva, J. Appl. Phys. **90**, 3396 (2001).
[29] O. Mitrofanov and M. Manfra, J. Appl. Phys. **95**, 6414 (2004).
[30] P. Maksymovych, M. Pan, P. Yu, R. Ramesh, A. P. Baddorf, and S. V. Kalinin, Nanotechnology **22**, 254031 (2011).
[31] P. Maksymovych, A. N. Morozovska, P. Yu, E. A. Eliseev, Y.-H. Chu, R. Ramesh, A. P. Baddorf, and S. V. Kalinin, Nano Lett. **12**, 209 (2012).
[32] E. A. Eliseev, A. N. Morozovska, G. S. Svechnikov, P. Maksymovych, and S. V. Kalinin, Phys. Rev. B **85**, 045312 (2012).
[33] M. D. Pickett, G. Medeiros-Ribeiro, and R. S. Williams, Nat. Mater. **12**, 114 (2013).
[34] M. P. Cosgriff, P. Chen, S. S. Lee, H. J. Lee, L. Kuna, K. C. Pitike, L. Louis, W. D. Parker, H. Tajiri, S. M. Nakhmanson, J. Y. Jo, Z. Chen, L. Chen, and P. G. Evans, Adv. Electron. Mater. **2**, 1500204 (n.d.).
[35] J. Jiang, Z. L. Bai, Z. H. Chen, L. He, D. W. Zhang, Q. H. Zhang, J. A. Shi, M. H. Park, J. F. Scott, C. S. Hwang, and A. Q. Jiang, Nat. Mater. **17**, 49 (2018).
[36] S. Farokhipoor and B. Noheda, Phys. Rev. Lett. **107**, 127601 (2011).
[37] P. Bednyakov, T. Sluka, A. Tagantsev, D. Damjanovic, and N. Setter, Adv. Mater. **28**, 9498 (2016).
[38] T. Sluka, A. K. Tagantsev, P. Bednyakov, and N. Setter, Nat. Commun. **4**, 1808 (2013).
[39] B. Sturman, E. Podivilov, M. Stepanov, A. Tagantsev, and N. Setter, Phys. Rev. B **92**, 214112 (2015).